ACS APPLIED MATERIALS & INTERFACES

Research Article

www.acsami.org

Helical TiO_2 Nanotube Arrays Modified by $Cu–Cu_2O$ with Ultrahigh Sensitivity for the Nonenzymatic Electro-oxidation of Glucose

Qian Yang,[†,‡,#] Mei Long,[†,#] Lin Tan,[†] Yi Zhang,[§] Jin Ouyang,[§] Ping Liu,[†] and Aidong Tang*[,†]

[†]School of Chemistry and Chemical Engineering, Central South University, Changsha 410083, China

[‡]Department of Neuroscience, Physiology, and Pharmacology, University College London, Gower Street, London WC1E 6BT, U.K.

[§]Department of Inorganic Materials, School of Resources Processing and Bioengineering, Central South University, Changsha 410083, China

Supporting Information

ABSTRACT: A novel $Cu–Cu_2O/TiO_2/Ti$ electrode for the nonenzymatic electro-oxidation of glucose has been fabricated by secondary anodic oxidation combined with the electrodeposition method. It represents a new type of copper oxide–TiO_2 complex nanostructure that demonstrates a new application. At the potential range from −1.0 to −1.6 V, Cu^{2+} was electrochemically reduced to Cu_2O, accompanied by the simultaneous formation of Cu covering the top surface of the TiO_2 nanotubes. The highest response current was obtained at the optimized fabrication conditions with a deposition charge of 1.5 C, a pH of 12, 4 mM $CuSO_4$, and a deposition potential of −1.4 V. The results indicate that Cu_2O helps to keep a broad linear range, and the incorporation of Cu nanoparticles improves the response current and sensitivity. The linearity between the response current and the glucose concentration was obtained in the range from 0.1 to 2.5 mM with a sensitivity of 4895 $\mu A\ cm^{-2}\ mM^{-1}$. Such high sensitivity was attributed to the synergistic effect of the small $Cu–Cu_2O$ grain size and the large surface area of the helical TiO_2 nanotube arrays as well as the fast electron transfer. Electrochemical impedance spectroscopy has been successfully applied to explain the differences among different electrode interfaces and the change rule of nonenzymatic electro-oxidation properties.

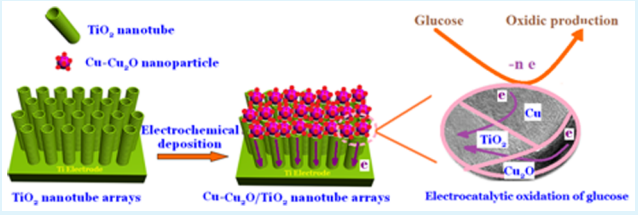

KEYWORDS: *Cu–Cu$_2$O nanoparticles, TiO$_2$ nanotube arrays, sensor, nonenzymatic electro-oxidation of glucose, electrochemical impedance spectroscopy*

1. INTRODUCTION

The fast and reliable determination of glucose has attracted extensive attention due to the need for the regular monitoring of blood glucose concentration for the increasing number of individuals with diabetes and the need for monitoring glucose concentration in bioindustrial processes, quality control, and glucose biofuel cells. Numerous efforts have been devoted to constructing various glucose sensors since Clark[1] and Updicke[2] reported the first enzyme electrode 50 years ago. Despite the fact that enzyme-based biosensors show good selectivity and high sensitivity, they are limited by their instability, complex enzyme immobilization, and high sensitivity to temperature, pH, and humidity.[3] To overcome these drawbacks, researchers have intensively explored the nonenzymatic electro-oxidation of glucose over different substrates such as platinum,[4,5] gold,[6,7] Ni,[8] and alloy.[9] However, most of these electrodes were found to suffer the problems of low sensitivity and poor selectivity caused by surface poisoning from the absorbed intermediates and the interference from chloride, ascorbic acid, uric acid, and dopamine. Nanomaterial-based nonenzymatic biosensors promise to solve these problems and show significantly higher sensitivity than enzymatic systems.[10] It has been reported that the sensitivity, selectivity, and antifouling properties can be improved by increasing the ratio of the nanoscopic surface area to the geometric surface area (roughness factor) because nanomaterials impose a very high active surface area that is significantly greater than the geometric surface area and is ideal for a kinetically controlled reaction.[11,12] The effective components, such as noble metals (Au, Pd, and Pt) and their alloys (Au–Pt and Pt–Pd), transition metal (Ni and Cu) and their oxides (NiO, CuO, and Cu_2O),[13] complexes (cobalt phthalocyanine tetrasulfonate, nickel hexacyanoferrate, etc.),[10] were usually deposited onto conducting substrate to improve the oxidation rate and stability of the active materials. Among these materials, Cu (especially Cu_2O) was extensively investigated for the electro-oxidation of glucose.[14] Many kinds of Cu-based sensors were prepared by modifying electrodes with Cu_xO nanoparticles, such as Cu_2O–straight multiwalled carbon nanotube hybrid nanostructures and Cu_xO nanoparticles deposited on polypyrrole nanowires.[15,16] However, Cu_2O, as a typical p-type transition metal oxide, has poor

Received: February 15, 2015
Accepted: May 13, 2015
Published: May 13, 2015

DOI: 10.1021/acsami.5b03401
ACS Appl. Mater. Interfaces 2015, 7, 12719−12730

conductivity[17] that is not favorable for charge transfer as a glucose sensor.

TiO_2 nanotube arrays (NTA) are commonly used to load catalysts for glucose electrocatalytic oxidation because of their unique physical and chemical properties, such as their excellent biocompatibility, nontoxicity, good chemical and thermal stability, well-aligned nanostructures with good adhesion to the substrate, and their preference for catalysts adsorbed onto the surface of both sides of nanotubes that retain a highly specific surface area.[8,18] Therefore, various metal oxides have been combined with TiO_2 to produce a synergistic effect, which has not only improved the catalytic activity and enhanced the stability of the metal oxides but also prevented the aggregation of the metal oxides. Until now, many approaches have been demonstrated to synthesize metal oxides−TiO_2 hybrids.[14,19−23] Among them, electrodeposition is one of the most convenient and effective methods for depositing Cu_xO nanoparticles onto the TiO_2 NTA structure. For example, Luo et al.[14] fabricated CuO/TiO_2 NTA nanofibers using dipping methods. Huang et al.[21] systemically studied the influence of electrochemical parameters on the formation of octahedral Cu_2O. It was found that octahedral Cu_2O particles were obtained under a larger deposition current, and amorphous Cu_2O was obtained under a smaller current at reduction potentials (−0.50 to approximately −0.20 V) referenced to Ag−AgCl. However, during the process of electrodeposition, the prompt growth of Cu_xO nanoparticles remained a big challenge for improving the catalytic activities and sensitivities of Cu-based nanoparticle glucose sensors. Recently, the loading of Cu and Cu oxide nanoparticles on TiO_2 catalyst has enhanced the photocatalytic H_2 reduction.[24,25] Additionally, multicomponent Cu−Cu_2O/TiO_2 nanojunction systems, which lead to better photocatalytic performance, were synthesized by a mild chemical process.[26,27] The Cu metal core is believed to play a key role in the enhancement of photocatalytic properties of Cu_2O−Cu/TiO_2 nanotube heterojunction arrays.[27] Cu_2O is fabricated on a TiO_2 flat surface using a special interrupted pulse electrodeposition, and significant enhancement of the photoelectrochemical activity is obtained when Cu_2O or Cu particles cover the TiO_2 surface.[28] The above cases demonstrate that improvement of photocatalytic properties is reasonable for semiconductors because the match of the energy bands of Cu_2O and TiO_2 facilitate the separation of the photogenerated charge and hole. However, what is the reason for the enhancement of the electro-oxidation activity given that there is no photogenerated charge and hole in the Cu-based TiO_2 glucose sensor? The nonenzymatic electro-oxidation of glucose processes are affected by surface properties and can be controlled by modifying the surface of TiO_2. Although to date, most studies on surface-modified TiO_2 have used single components such as in Ni/TiO_2, Pt/TiO_2, and Cu_2O/TiO_2, there is still no report on the fabrication of Cu−Cu_2O nanoparticles on the surface of TiO_2 NTA as a transducer for a nonenzymatic glucose sensor. According to Ortiz's assumption,[29] glucose is oxidized on the Cu or Cu composite electrodes in an alkaline medium through a reaction with CuOOH to form $Cu(OH)_2$:

$$\mathrm{CuOOH} + \mathrm{glucose} \leftrightarrow \mathrm{Cu(OH)_2} + \mathrm{oxidation\ products} \quad (1)$$

The oxidation processes are catalyzed by the Cu-based sensors through the formation of a highly valent oxyhydroxide species (CuOOH) in an alkaline medium.[30] However, it is clear that investigating isolated materials is no longer sufficient to solve all kinds of technological challenges for the development of high-performance glucose sensors. The synergic effect of two surface modifiers should be larger than the sum of the single-component effects, which implies that both modifiers together enhance the overall direct electrocatalytic oxidation. Therefore, researchers should pay great attention to the fabrication technique when investigating the interface contact between individual components within a system. Herein, on the basis of our previous work,[3] it is proposed that in new work two surface modifiers, Cu_2O and Cu, are simultaneously assembled onto the helical-like TiO_2 nanotubes by an easy electrodeposition method. As the TiO_2 nanotubes with helical-like morphology were successfully prepared and reported in our previous work,[3] it will be propitious to the mass transport and transfer charge to enhance the glucose electrocatalytic activity. Introducing Cu is beneficial to the conductivity of the electrode, and the deposit of Cu nanoparticles on Cu_2O is also important to prevent Cu_2O nanoparticles from growing. The fabrication process has two main steps: The first step is the anodic growth of helical TiO_2 NTA from a Ti foil following calcinations at 500 °C. The as-obtained helical-like TiO_2 NTA favor rapid mass transport. In the second step, the Cu-based nanoparticles are electrodeposited on the surface of the TiO_2 NTA at a constant potential range from −1.0 to −1.6 V. This potential range is more negative than in most reports in the literature.[31,32] The Cu−Cu_2O/TiO_2 NTA/Ti electrode displayed high sensitivity, faster response, and a broad linear range for glucose detection. For constructing the relationship between the Cu-based oxide and the performance of glucose catalytic oxidation, the effect of the electroplating condition on the property of the electrocatalytic oxidation of glucose over the Cu−Cu_2O/TiO_2 NTA/Ti electrode was also carefully studied by X-ray diffraction (XRD), scanning electron microscopy (SEM), transmission electron microscopy (TEM), cyclic voltammetry (CV), and electrochemical impedance spectroscopy (EIS). The detailed EIS results explain well the characteristics of the electrochemical reaction at the interface.

2. EXPERIMENTAL SECTION

2.1. Chemicals. All chemicals used in this study were of analytical grade. Glucose, $CuSO_4{\cdot}5H_2O$, NaOH, NH_4F, glycerol, lactic acid, and Ti foils (purity >99.6%) were purchased from commercial sources in China and used as received. Double-distilled water was used for the preparation of standard solutions.

2.2. Preparation of the Cu−Cu_2O/TiO_2 NTA Electrode. TiO_2 NTA were fabricated through a two-step anodization. Before fabrication, Ti foils (purity >99.6%, 100 × 10 mm in size, 0.14 mm in thickness) were ultrasonically cleaned in water. The Pt foil (purity >99.9%) was used as the cathode, and the pure Ti foil was used as the anode. A potentiostat (YB 1711 type, China) was used as the power source. In the first step, anodization was carried out in a glycerol electrolyte containing 0.5 wt % NH_4F. The voltage and oxidation time was 20 V and 1 h, respectively. Afterward, the preanodized Ti foil was ultrasonically cleaned in water to remove the formed TiO_2 film. The cleaned Ti foil was used for secondary anodization in a similar electrolyte. The voltage and oxidation time were 20 V and 3 h, respectively. The as-prepared TiO_2 nanotubes were cleaned using distilled water, air-dried, and then calcined in a muffle furnace at 500 °C for 3 h.

Cu−Cu_2O/TiO_2 NTA composites were prepared by the electrochemical deposition of Cu and Cu_2O in a three-electrode cell using the TiO_2 NTA electrode, saturated calomel electrode (SCE), and platinum foil as the working, reference, and counter electrodes, respectively. The electrolyte was obtained by dissolving $CuSO_4$ in 3 mol L^{-1} lactic acid solution to form a copper lactate complex, and the pH was adjusted to

DOI: 10.1021/acsami.5b03401
ACS Appl. Mater. Interfaces 2015, 7, 12719−12730

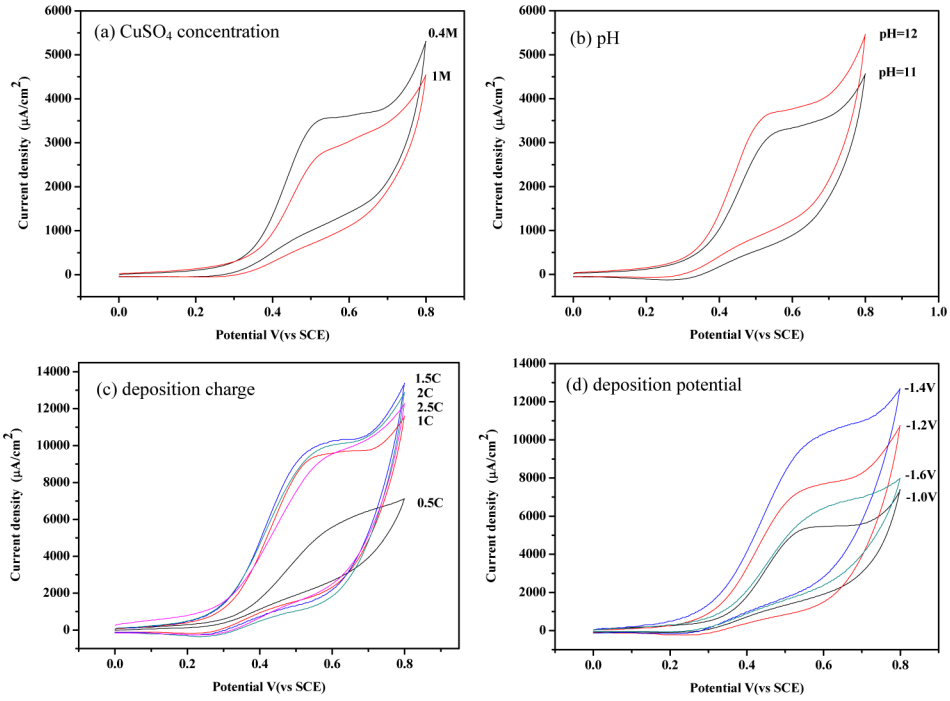

Figure 1. CV curves of different Cu−Cu_2O/TiO_2 NTA/Ti electrodes prepared at different (a) $CuSO_4$ concentrations, (b) pH, (c) deposition charges, and (d) deposition potentials in the presence of 2 mM glucose in 0.10 M NaOH. Note: when one of the conditions is changed, other conditions stay the same (0.4 M $CuSO_4$ solution, pH 12, charge of 1.5 C, and potential of −1.4 V).

11 or 12 using 5 M NaOH solution. The electrolyte was stirred and kept at a constant temperature of 35 °C. The electrodeposition charge range selected from 1 to 2.5 C was used during the deposition process. Cu and Cu_2O particles were coated on the TiO_2 NTA by electrochemical deposition. The electrodeposition potential was kept between −1.0 and −1.6 V (versus SCE) for 40−100 s by controlling the deposition charge. All the potentials in this paper were based on SCE reference electrodes.

2.3. Characterization. XRD patterns of the fabricated products were recorded on a DX-2700 X-ray diffractometer (Liaoning Dandong Hao Yuan Instruments Co., Ltd) at a scan rate of 0.05° s^{-1} with a 2θ range from 20 to 80 °C using high-intensity Cu Kα radiation (λ = 0.15418 nm). Images were obtained using the FEI Nova NanoSEM 230 field emission SEM. Microstructures and morphologies were investigated using the Tecnai G^2 F20 S-TWIN (FEI Company) TEM with a field emission gun of 200 kV.

2.4. Electrochemical Measurements. The electrochemical performance of the Cu−Cu_2O/TiO_2 NTA/Ti electrode for detection of glucose was investigated by CV, chronoamperometry, and EIS. Electrochemical measurements were performed on a CHI 660B electrochemical workstation (ChenHua Instruments Co. Ltd, Shanghai, China) with a conventional three-electrode setup, with Cu−Cu_2O/TiO_2 NTA/Ti as the working electrode, Pt foil as the counter electrode, and SCE as the reference electrode. Using the modified Cu−Cu_2O/TiO_2 NTA/Ti working electrode, data from the CV experiments and the amperometric experiments were measured in a mixture of 2 mmol L^{-1} glucose and 0.1 mol L^{-1} NaOH solutions. The CV measurements required the operation of the electrode in a range of potentials from 0 to 0.8 V versus SCE. The amperometric curve measurements required the operation of the electrode at a constant applied potential from 0.40 to 0.70 V versus SCE. Once the current reached a baseline in the absence of glucose, glucose was added every 50 s thereafter. A magnetic stirrer and a stirring bar provided convective mass transport. EIS measurements were also performed in 0.1 M NaOH solution at an applied potential of +0.6 V in the frequency range of 0.1−10 MHz with a potential amplitude of 5 mV and plotted in the form of complex plane diagrams (Nyquist plots).

3. RESULTS AND DISCUSSION

3.1. Effects of Preparation Conditions on the Performance of Glucose Nonenzymatic Electro-oxidation over Cu−Cu_2O/TiO_2 NTA/Ti Electrodes. The fabrication process has two main steps: The first step is the anodic growth of helical TiO_2 NTA from a Ti foil following calcinations at 500 °C according to the literature.[3] Figure S1 in the Supporting Information shows the XRD pattern and the SEM image of the annealing-treated TiO_2 NTA electrode. The peaks at 2θ = 25.44, 48.16, and 55.14°, shown in Figure S1A of the Supporting Information, are attributed to the diffraction peaks of anatase TiO_2 (JCPDS file: 21-1272). It can be seen that the TiO_2 NTA has an average diameter of about 105 nm and tube length of about 300 nm in Figure S1B in the Supporting Information. The as-obtained helical-like TiO_2 NTA favor rapid mass transport because the average apparent heterogeneous electron transfer rate constant (k) was 2.18 × 10^{-3} cm s^{-1} for TiO_2 NTA modified by surface defects, which can match the electron transfer rate constant of carbon nanotubes (7.53 × 10^{-4} cm s^{-1}).[8] In the second step, to obtain a suitable Cu- and Cu_2O-modified TiO_2 layer, Cu and Cu_2O were potentiostatically deposited on the above-obtained TiO_2−Ti specimen by employing different electroplating conditions. The effects of several factors that mainly influence electrodepositing, such as $CuSO_4$ concentration, pH, deposition charge, and potential on the catalytic activity, were investigated by means of CV technique. The Cu-based nanoparticles are electrodeposited on the surface of the TiO_2 NTA at a constant potential range from −1.0 to −1.6 V. These more negative potentials employed in this study have never been considered before, although it was reported that the electrochemical deposition was carried out at a potential of −0.8 V referenced to Ag−AgCl.[31,32]

DOI: 10.1021/acsami.5b03401
ACS Appl. Mater. Interfaces 2015, 7, 12719−12730

The CV curves of different Cu−Cu_2O/TiO_2 NTA/Ti electrodes prepared at different conditions were compared, as shown in Figure 1. It was found that the Cu−Cu_2O/TiO_2 NTA/Ti electrodes showed obvious catalytic oxidation in the presence of 2.0 mM glucose in 0.1 M NaOH solution. The lower oxidation peak potential and higher response current represent better electrocatalytic activity. These results showed that the Cu−Cu_2O/TiO_2 NTA/Ti electrodes have good electrocatalytic activity toward the oxidation of glucose. By comparing the effects of the electroplating conditions, such as comparing the effects of the solution pH values and $CuSO_4$ concentrations on the property of glucose enzyme-free oxidation, we found that the response current was higher for 0.4 M $CuSO_4$ than for 1 M $CuSO_4$ (see Figure 1a), and the response current was greater at pH 12 than at pH 11 (see Figure 1b).

In contrast, the effects of deposition potential and charge were more significant (shown in Figure 1c,d). After a comparison of the deposition charge effect on the performance of the sensor, it was found that the response current for glucose oxidation increased rapidly when the deposition charge increased from 0.5 to 1.5 C (see Figure 1c). However, when the deposition charge was increased to 2.5 C, the response current to glucose oxidation slowly decreased. The results clearly demonstrated that the optimum deposition charge is 1.5 C. In contrast, the influence of the deposition potential was the largest among the four preparation conditions. It was found that as the deposition potential increased to −1.2 V, the response current for glucose oxidation increased rapidly. The largest response current was obtained at the deposition potential of −1.4 V, in 0.4 M $CuSO_4$ solution, at pH 12, and at a charge of 1.5 C as shown in Figure 1d. The oxidation current rapidly increased, starting around 0.32 to 0.37 V with the appearance of an oxidation peak around 0.54 V and finishing around 0.70 V. The starting oxidation potentials were different for 0.32, 0.34, 0.36, and 0.37 V for the electrodes prepared at −1.4, −1.2, −1.0, and −1.6 V, respectively. Furthermore, from the CV results, it was found that the glucose nonenzymatic biosensor based on the Cu−Cu_2O/TiO_2 NTA/Ti electrode provides not only a prominent augmentation of response current toward glucose but also a relatively low oxidation potential of 0.54 V.

3.2. Structure and Morphology Comparisons with Electrodes Prepared at Different Deposition Potentials.

For understanding the effects of the deposition potential on the property of electrocatalytic oxidation of glucose over Cu−Cu_2O/TiO_2 TNA/Ti sensors, the structures and morphologies of the sensors were carefully investigated by means of XRD, SEM, and TEM.

Figure 2A shows the XRD patterns and the SEM images of the samples prepared at different deposition potentials. The observed diffraction peaks can be assigned to Cu_2O, Cu, anatase TiO_2, and Ti substrate. Thus, the XRD pattern demonstrates that the as-synthesized samples are composites consisting of Cu, Cu_2O, and anatase TiO_2.

The presence of Cu_2O in the sample after deposition can be confirmed by the characteristic diffraction peaks at 36.5°, assigned to the (111) crystal planes of the cubic Cu_2O (JCPDS file: 65-3288). It was noted that the intensity of the peak at 36.5° decreased when the electroplating potential changed from −1.0 to −1.6 V, indicating that the amount of Cu_2O had decreased. Meanwhile, the diffraction patterns clearly show two major peaks at 43.50 and 50.50° in the range of 20−80°, which

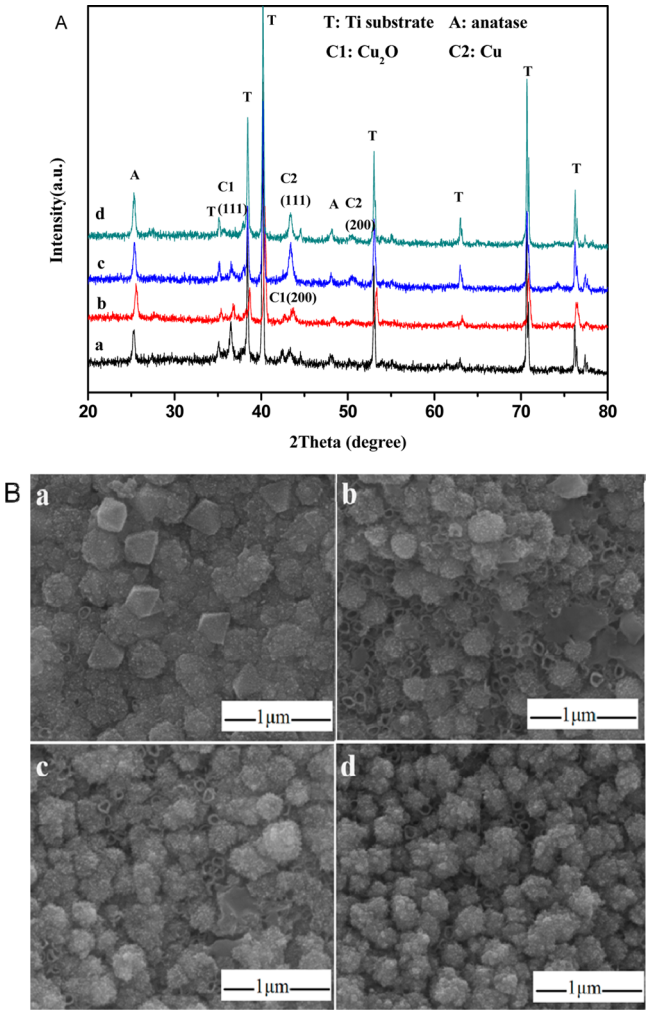

Figure 2. (A) XRD patterns and (B) SEM images of Cu−Cu_2O/TiO_2 TNA/Ti samples prepared at different electrodeposition potentials: (a) −1.0 V; (b) −1.2 V; (c) −1.4 V; and (d) −1.6 V in 0.4 M $CuSO_4$ solution at pH 12 with a charge of 1.5 C.

were assigned to the diffraction from the (111) and (200) planes of the face-centered cubic lattice of Cu(0) (JCPDS file: 04-0836), respectively. The characteristic peaks of Cu appeared when the deposition potential was greater than −1.0 V, and the intensity increased gradually with the increase of deposition potential from −1.0 to −1.4 V, indicating the amount of Cu nanoparticles deposited on the electrode surface was increasing. It can be seen that the peak of the Cu (111) plane reflection is the strongest for the electrode prepared at a potential of −1.4 V. The peak of the Cu (111) plane reflection for the electrode prepared at a potential of −1.6 V is lower than that for the electrode prepared at a potential of −1.4 V. The growing Cu and Cu_2O nanoparticles on TiO_2 NTA yielded Cu−Cu_2O/TiO_2 NTA composites with a three-dimensional ordered structure, which may provide an ideal interface for application in an electrochemical sensor.

Figure 2B shows the SEM images of the obtained electrodes deposited at different potentials. It can be seen that the surface of the TiO_2 NTA was completely covered by Cu−Cu_2O nanoparticles with diameters of 200−300 nm after 20−50 s, forming the Cu−Cu_2O/TiO_2 NTA composite. The thickness of the Cu−Cu_2O layer is about 50−100 nm. The octahedral particles with (111) crystal facets appeared mainly at the

DOI: 10.1021/acsami.5b03401
ACS Appl. Mater. Interfaces 2015, 7, 12719−12730

electrodeposition potential −1.0 V. In contrast, it is noted that the surfaces of the Cu−Cu_2O particles at −1.0 and −1.4 V were smoother than the surfaces of the Cu−Cu_2O particles at −1.6 and −1.2 V in Figure 2B. The octahedral Cu_2O particles with side lengths of 200−300 nm covered the top surface of the tubular structures in Figure 2B, panel a. It was noted that the octahedral Cu_2O particles disappeared when the potential was −1.2 V. This result demonstrated that introducing Cu by applying more negative potential effectively prevented Cu_2O from growing.

This was clarified by a Scherrer equation calculation of the grain sizes[33] in Figure 3. The grain sizes of the (111) crystal

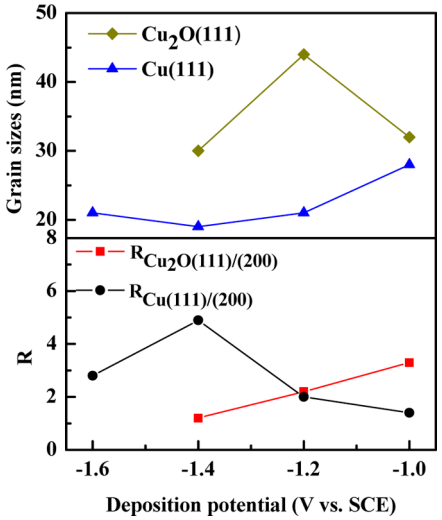

Figure 3. Grain sizes and ratios $R_{(111)/(200)}$ of Cu and Cu_2O in samples prepared at different electrodeposition potentials.

plane of Cu_2O and Cu were calculated at about 32, 44, and 30 nm and 28, 21, and 19 nm for the samples prepared at −1.0, −1.2, and −1.4 V, respectively. It was found that the samples prepared at −1.4 V presented the minimum crystal sizes for both Cu_2O and Cu particles. Combining the CV results in Figure 1d, it demonstrates that the starting oxidation potential is highly dependent on Cu_2O and Cu grain size, and the best data were obtained from a Cu grain size of 19 nm from the Scherrer equation calculation.

The shapes of the cubic crystals for Cu_2O and Cu are determined by the growth ratio, R, of the growth rate along the (111) directions to the (200) directions in Figure 3. From the general trend, $R_{(111)/(200)}$ of Cu_2O shows a significant decline, and $R_{(111)/(200)}$ of Cu presents an increasing trend. Although the value of $R_{(111)/(200)}$ of Cu at −1.6 V is smaller than that at −1.4 V, it is bigger than that at −1.2 and −1.0 V. When the deposit potential is −1.0 V, the driving force for Cu_2O formation is greater than that for Cu formation. Therefore, octahedral Cu_2O quickly forms, with a corresponding R_{Cu_2O} of 3.3 and R_{Cu} of 1.4.

As the potential increases, the corresponding decrease of the driving force for Cu_2O formation confines the growth of Cu_2O rather than facilitating the growth of Cu. The R_{Cu_2O} is 1.2 while the R_{Cu} is 4.9 when the potential increases to −1.4 V. It is noted that the (111) face of Cu is very significant in Figure 2A. When the potential continues to increase to −1.6 V, both Cu_2O and Cu grow quickly, resulting in the formation of smaller Cu_2O and Cu; although the peak of Cu_2O cannot be identified (but Cu_2O can be seen in high-resolution transmission electron microscopy (HRTEM) in Figure 4d), the R_{Cu} obviously becomes small. On the basis of the above experimental results and analysis, there should be a strong interaction between the surfaces of the Cu_2O and Cu particles, although the properties of the electrodes with different ratios of Cu_2O and Cu still need to be studied further.

TEM and HRTEM images of the obtained Cu−Cu_2O/TiO_2 NTA/Ti samples prepared at different electrodeposition potentials are shown in Figure 4. Referring to SEM images, Cu and Cu_2O are surely produced together and basically on the surface, which is further confirmed by the TEM and HRTEM images of the synthesized samples (Figure 4).

The TEM images show that the synthesized samples consist of nanoparticles with irregular shapes around 20−30 nm, and the TiO_2 nanotubes possess thicknesses of about 10 nm. In particular, the helical-like TiO_2 is clearly presented in Figure 4b−d. The HRTEM images show the lattice fringes arising from Cu, Cu_2O, and TiO_2. A lattice fringe of 0.352 nm is consistent with the (101) planes of anatase TiO_2. A lattice fringe with a length of 0.246 nm matches well with (111) planes of cubic Cu_2O, and a lattice fringe with a length of 0.209 nm matches well with (111) planes of cubic Cu. Generally, TEM and HRTEM images demonstrate that Cu and Cu_2O truly exist but cannot demonstrate whether the Cu and Cu_2O is on the surface or in the tubes because this is not in situ TEM. However, TEM and HRTEM images demonstrate that TiO_2 nanotube arrays have helical morphology. Combined with the CV, XRD, and TEM results, the improvement in electrocatalytic activity for the oxidation of glucose on the Cu−Cu_2O/TiO_2 NTA/Ti electrode in an alkaline medium can be ascribed to the rational coupling of components and dimensional control.

3.3. Sensor Performance Comparisons of the Electrodes Prepared at Different Deposition Potentials. To clarify the performance of the Cu−Cu_2O/TiO_2 NTA/Ti sensors prepared at different potentials, we adopted chronoamperometry to investigate the direct electrocatalytic oxidation of glucose on the Cu−Cu_2O/TiO_2 NTA/Ti electrode in an alkaline medium. Upon each addition of 0.5 mM glucose, the solution was stirred constantly and the electrochemical response recorded. The current increased as the concentration of glucose increased, as shown in Figure S1 in the Supporting Information. Compared with the effect of the different deposition potentials on the electro-oxidation of glucose, the Cu−Cu_2O/TiO_2 NTA/Ti electrodes prepared at −1.4 and −1.2 V present obvious high-response currents. A high current is favorable to enhance the sensitivity of the biosensors.

The parameters and results calculated from the corresponding calibration curves are shown in Table 1. The linear ranges lessen as the deposition potential increase within the range from −1.0 to approximately −1.6 V with linear dependence beyond 0.99. The more negative the deposition potential that is controlled, the smaller the linear range obtained. A maximum linear calibration curve for glucose determination is obtained in the concentration range of 0.1−4 mM, with a detection limit of 8.4 μM when the preparation of reduction potential is −1.0 V. For Cu−Cu_2O/TiO_2 NTA/Ti electrodes, the low deposition potential is useful for getting a wide linear range. For comparison of the linear calibration curves for glucose determination, we calculated the slope according to the amperometric response curves to glucose, which indicated that the electrodeposition potential of −1.4 V would be

DOI: 10.1021/acsami.5b03401
ACS Appl. Mater. Interfaces 2015, 7, 12719−12730

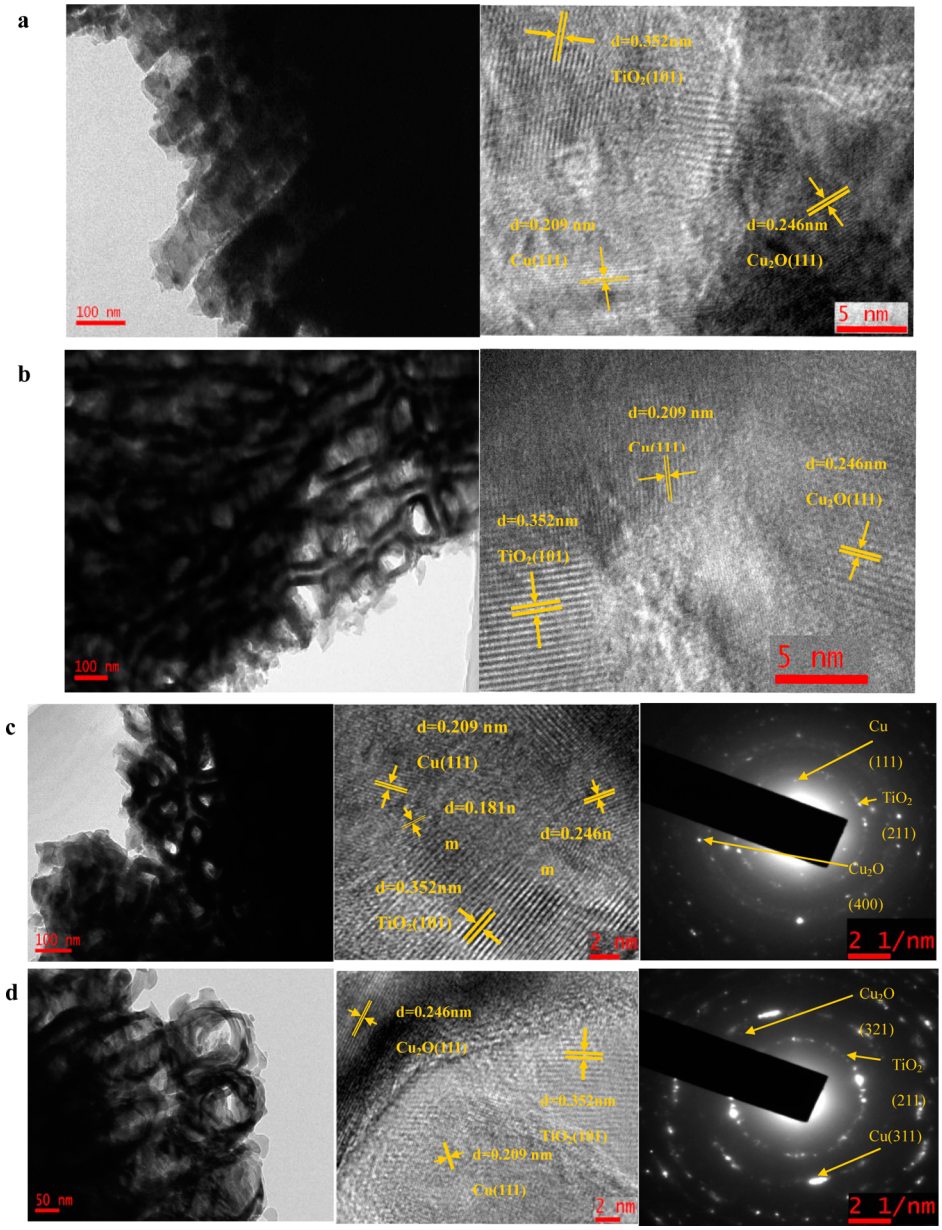

Figure 4. TEM images of Cu−Cu_2O/TiO_2 NTA/Ti samples prepared at different electrodeposition potentials (a) −1.0, (b) −1.2, (c) −1.4, and (d) −1.6 V.

Table 1. Comparison of the Performance of the Cu−Cu_2O/TiO_2 NTA/Ti Electrode Prepared at Different Deposition Potentials

deposition potential (V)	linear range (C/mM)	sensitivity (μA mM^{-1} cm^{-2})	correlation coefficient	detection potential (V vs SCE)	detection limit (μM)
−1.0	0.1−4.0	2961	0.994	0.6	8.4
−1.2	0.1−3.0	3884	0.991	0.6	6.0
−1.4	0.1−2.5	4346	0.989	0.6	8.6
−1.6	0.1−1.5	4070	0.994	0.6	9.8

favorable for a Cu−Cu_2O/TiO_2 NTA/Ti electrode with a high sensitivity for detecting glucose. The sensitivity of the composite electrodes could reach a value as high as 4346 μA mM^{-1} cm^{-2}, and the detection limit was about 8.6 μM with a signal-to-noise ratio of 3 (S/N = 3). The above results indicate that Cu_2O helps to keep a broad linear range, and the incorporation of Cu nanoparticles favors improvement in the response current and sensitivity.

EIS is a powerful technique for studying the interface properties of electrode surfaces. To further explain the effect of different electrodeposition potentials on the performance of the sensor, we present the Nyquist plots of the different electrodes in Figure 5.

The EIS of all samples included a semicircle portion observed in the higher frequency range, representing the electron-transfer-limited process, and a linear segment at lower frequencies, representing the diffusion-limited process. Impedance spectra were analyzed by fitting them to the equivalent electrical circuits using ZView software (Scribner Associates, USA). The complex spectrum was found to fit well with the

DOI: 10.1021/acsami.5b03401
ACS Appl. Mater. Interfaces 2015, 7, 12719−12730

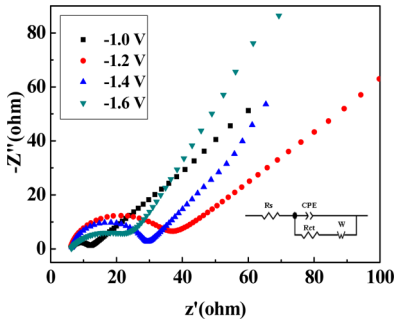

Figure 5. Nyqist plots of the EIS of the Cu−Cu_2O/TiO_2 NTA/Ti electrode prepared at different deposition potentials (−1.0, −1.2, −1.4, and −1.6 V) for glucose nonenzymatic oxidation in 0.10 M NaOH containing 2 mM glucose at an applied potential of 0.6 V. The inset is a modified Randle's equivalent circuit.

modified Randle's circuit, in which the double layer capacitance (C_{dl}) was replaced by a constant phase element (CPE), modeled as a nonideal capacitor. The schematic representation of the modified Randle's equivalent circuit for this Cu−Cu_2O/TiO_2 NTA/Ti electrode is shown in the inset in Figure 5. The EIS parameters for the electron transfer characteristics of the different electrodes are listed in Table 2. Significant differences in the impedance spectra are observed.

Table 2. Equivalent Circuit-Fitting Data from Impedance at the Cu−Cu_2O/TiO_2 NTA/Ti Electrode Prepared at Different Deposition Potentials[a]

	deposition potential (V)			
	−1.0	−1.2	−1.4	−1.6
Rs (Ω cm^2)	6.4	6.0	6.4	6.2
CPE-T ($10^6 \mu F\ cm^{-2}\ s^{n-1}$)	13.1	11.8	11.8	71.8
CPE-P	0.90	0.88	0.91	0.66
Rct (Ω cm^2)	5.2	28.3	22.2	20.0
W-R (Ω cm^2)	175	336	172	486
W-T (s)	9.0	9.4	7.6	12.3
W-P	0.50	0.48	0.58	0.71

[a]The EIS spectra were recorded at +0.60 V versus SCE.

The capacitance CPE-T describes the charge separation at the double layer interface, and the exponent CPE-P is due to the heterogeneity of the surface. Zw was modeled as an open circuit finite Warburg element, as already used for other modified electrodes.[34] W-R is the diffusion resistance of electroactive species, W-T is a time constant depending on the diffusion rate, and W-P = 0.5 is for a perfect uniform flat interface. Values of W-P of less than 0.5 express the fact that the interface is not uniform. The diameter of a semicircle portion is equal to the electron transfer resistance (Rct), which reflects conductivity and is related to the electron transfer kinetics of the redox reaction at the electrode surface. Rs represents the resistance of electrolyte solution.[34]

The capacitance CPE-T increases to 71.8×10^{-6} $\mu F\ cm^{-2}\ s^{n-1}$, and CPE-P is 0.66 for the electrode prepared at −1.6 V, indicating that the ability of charge separation at the double layer interface is improved, but the heterogeneity of the surface is worse due to the deposition potential being more negative. More importantly, it is found that the heterogeneity of the surface and the SEM image of a film present results consistent with each other. For example, the exponent CPE-P of the samples at −1.0, −1.2, −1.4, and −1.6 V are 0.90, 0.88, 0.91, and 0.66 (in Table 2), respectively. The exponents CPE-P (0.90 and 0.91) for −1.0 and −1.4 V are very close, and the exponents CPE-P (0.88 and 0.66) for −1.2 and −1.6 V are clearly become smaller. This result is consistent with the observation of SEM images in Figure 2B.

The Rct of electrodes prepared at different potentials was calculated to be 5.2−28.3 (Ω cm^2) and was relatively small, indicating that the electron transfer ability of these electrodes could be improved by depositing Cu−Cu_2O on the surface of the TiO_2 NTA-applied deposition potential from −1.0 to −1.6 V. The Warburg impedances W-R of the electrode prepared at −1.0 and −1.4 V were smaller than those of the electrode at −1.2 and −1.6 V, indicating that the diffusion resistances of electroactive species for the electrode prepared at −1.0 and −1.4 V were small due to the small grains of Cu_2O (30 and 32 nm for the samples at −1.0 and −1.4 V as calculated by the Scherrer equation) as shown in Figure 3B. W-T is a time constant depending on the diffusion rate, W-T = l^2/D, where l is the effective diffusion thickness, and D is the effective diffusion coefficient of the species.[35] By comparing the W-T values in Table 2, it is seen that the smallest W-T value is 7.6 s when obtained for the electrode prepared at −1.4 V, implying that the electrode has the most appropriate effective diffusion thickness and effective diffusion coefficient of the species.

3.4. Sensor Properties of the Cu−Cu_2O/TiO_2 NTA/Ti Electrode Prepared at −1.4 V. From the CV of Figure 1d, it is seen that the peak potential for the catalytic oxidation of glucose is maximized and reaches a constant value above 0.54 V. The potential can be fixed at any value in the constant current region of 0.54−0.7 V, and the determination of glucose in alkaline solution can be conveniently carried out. To evaluate the effect of different applied potentials on the performance of the amperometric sensor for the determination of glucose, we recorded the amperometric responses to glucose at the Cu−Cu_2O/TiO_2 NTA/Ti electrode prepared at −1.4 V, and the corresponding calibration curves are shown in Figure S2 in the Supporting Information. The amperometric response currents increase as the electrocatalytic oxidation potential increases. The linear ranges of electrocatalytic oxidation potentials in the range of 0.50−0.65 V were investigated. The parameters and results calculated from the corresponding calibration curves are shown in Table 3.

Table 3. Effects of Applied Potential on the Sensor Performance of the Cu−Cu_2O/TiO_2 NTA/Ti Electrode Prepared at −1.4 V

applied potential (V)	linear range (C/mM)	sensitivity ($\mu A\ mM^{-1}\ cm^{-2}$)	correlation coefficient
0.50	0.1−1.0	4405	0.994
0.55	0.1−1.5	4660	0.996
0.60	0.1−2.0	4580	0.993
0.65	0.1−2.5	4895	0.992

The linear ranges rise as the applied potential increases in the range of 0.50−0.65 V with the linear dependence beyond 0.99. It was found that the applied high potential is useful for getting a wide linear range. The sensitivity of the Cu−Cu_2O/TiO_2 NTA/Ti electrode can reach a value as high as 4895 $\mu A\ mM^{-1}\ cm^{-2}$ at an applied potential of 0.65 V. As shown in Table 3, the linear range and sensitivity increase with the increase of applied potential. It demonstrates that a higher applied potential is

DOI: 10.1021/acsami.5b03401
ACS Appl. Mater. Interfaces 2015, 7, 12719−12730

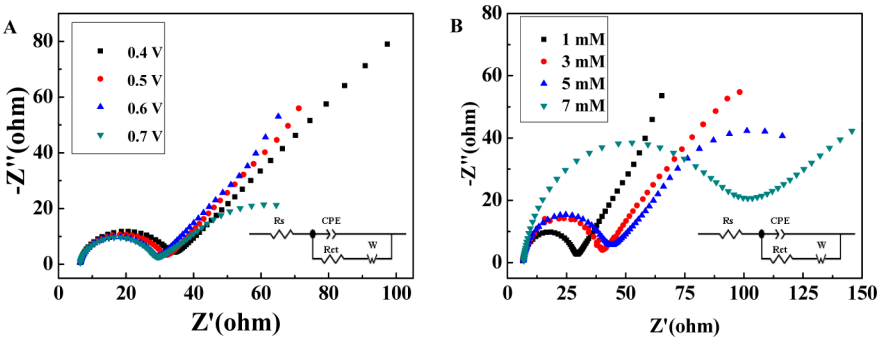

Figure 6. (A) Nyqist plots of the EIS of the Cu−Cu_2O/TiO_2 NTA/Ti electrode at different applied potentials (0.4, 0.5, 0.6, and 0.7 V) in 0.10 M NaOH containing 1 mM glucose. (B) Nyqist plots of the EIS of the Cu−Cu_2O/TiO_2 NTA/Ti electrode in 0.10 M NaOH containing different concentrations of glucose (1, 3, 5, and 7 mM).

needed to form more Cu^{3+} sites for the direct catalytic oxidation of glucose. However, a high potential can lead to more interference signals. An appropriate potential should be determined by compromising between the two factors. Thus, a suitable potential 0.6 V was selected. It can be concluded that the Cu−Cu_2O/TiO_2 NTA/Ti electrode can be used as an amperometric sensor for the determination of glucose with good sensitivity. As expected, the electrocatalytic activity of the Cu−Cu_2O/TiO_2 NTA/Ti electrode permits the convenient detection of glucose at lower potentials with high sensitivity.

The effect of the different applied potentials on the interface properties of electrode surfaces is shown in Figure 6A and Table 4. For the same electrode and electrolyte, the values of Rs and the CPE-P all remained constant as expected.

Table 4. Equivalent Circuit-Fitting Data from Impedance at the Cu−Cu_2O/TiO_2 NTA/Ti Electrode Prepared at −1.4 V[a]

	applied potential (V)			
	0.4	0.5	0.6	0.7
Rs (Ω cm^2	6.4	6.3	6.4	6.4
CPE-T ($10^6 \mu$F cm^{-2} s^{n-1})	11.6	14.0	11.8	10.7
CPE-P	0.91	0.90	0.91	0.92
Rct (Ω cm^2)	26.5	24.8	22.2	21.4
W-R (Ω cm^2)	475	250	177	58
W-T (s)	20.2	9.4	8.0	3.3
W-P	0.57	0.59	0.58	0.46

[a]The EIS spectra were recorded at different applied potentials.

The Rct of the electrode slightly decreased with increases in the applied potentials, which means that increasing the applied potentials could enhance the electron transfer ability of the electrode, leading to a higher conversion of glucose. Warburg impedances, W-R and W-T, obviously decrease with an increase of the applied potentials, indicating that the diffusion resistances of electroactive species decrease and the diffusion coefficient of electroactive species increase with an increase of the applied potentials. Overall, the high applied potentials favor the electrocatalytic oxidation of glucose.

An amperometric glucose sensor is based on the generation of electrons in catalyst-assisted glucose oxidation, resulting in a detectable current response that is linearly correlated with glucose concentration. To better understand the effect of the different glucose concentrations on the interface properties of the electrode surface, we present the results of the EIS in Figure 6B, Figure S3 in the Supporting Information, and Table 5.

Table 5. Equivalent Circuit-Fitting Data from Impedance at the Cu−Cu_2O/TiO_2 NTA/Ti Electrode Prepared at −1.4 V[a]

	glucose concentration (mM)			
	1	3	5	7
Rs (Ω cm^2)	6.3	6.5	6.6	6.8
CPE-T ($10^6 \mu$F cm^{-2} s^{n-1})	11.8	11.4	11.3	9.1
CPE-P	0.91	0.91	0.91	0.93
Rct (Ω cm^2)	22.2	31.6	34.4	78.9
W-R (Ω cm^2)	172	147	108	187
W-T (s)	7.6	4.7	2.6	1.7
W-P	0.58	0.50	0.48	0.38

[a]The EIS spectra were recorded at +0.60 V containing different concentrations of glucose.

Figure S2 in the Supporting Information shows that the catalytic oxidation current was proportional to the concentration of glucose in the range of 0.1−7.0 mM. The values of Rs in Table 5 slightly increased with the increase of the glucose concentration, and the values of Rct clearly increased with the increase of the concentration in the order of 1, 3, 5, and 7 mM. Rct significantly increases, especially when the concentration of glucose is 7 mM, showing that the adsorption of glucose on the electrode surface is approaching saturation and blocking the electron transfer at the interface. Meanwhile, the Warburg impedances (W-R and W-T) obviously decrease with an increase of the glucose concentration from 1 to 5 mM, indicating that the diffusion resistances of electroactive species decrease and the diffusion coefficient of electroactive species increase with an increase of the glucose concentration. However, as the glucose concentration approaches 7 mM, the W-R value significantly increases, which demonstrates that the diffusion of electroactive species is becoming difficult. In conclusion, for the electrocatalytic oxidation of glucose at the Cu−Cu_2O/TiO_2 NTA/Ti electrode in 0.10 M NaOH, the glucose concentration should be no more than 7 mM.

Figure 7 shows the CVs of the Cu−Cu_2O/TiO_2 NTA/Ti electrode recorded in 0.1 M NaOH solution containing 2 mM glucose at different scan rates. The oxidative peak current density at the corresponding potential 0.6 V is notably increased in a linear manner with the increasing scan rates in the range of 50−200 m V s^{-1} as shown in the inset of Figure 7. A good linearity between scan rate and peak current is obtained with i (μA/cm^2) = 5148 + 30.74ν (mV s^{-1}) and a correlation coefficient (R^2) of 0.98; i is the glucose oxidation peak current density, and ν is the scan rate. This behavior indicates that the oxidation of glucose at Cu−Cu_2O/TiO_2 NTA/Ti electrode is

DOI: 10.1021/acsami.5b03401
ACS Appl. Mater. Interfaces 2015, 7, 12719−12730

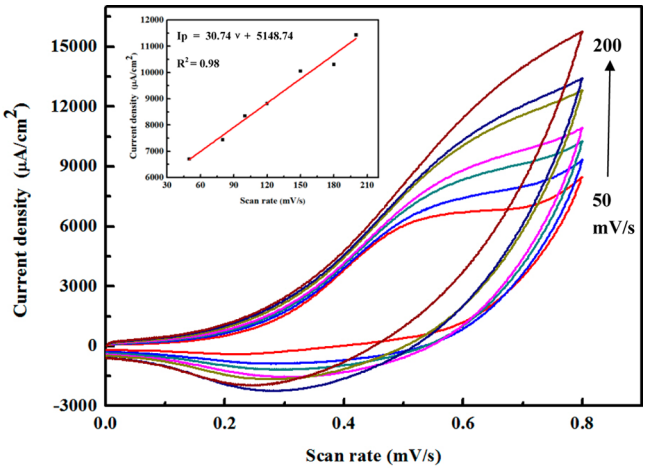

Figure 7. CVs of the Cu−Cu_2O/TiO_2 NTA/Ti electrode obtained in 0.10 M NaOH solution containing 2 mM glucose at different scan rates (inner to outer: 50, 80, 100, 120, 150, 180, and 200 mVs^{-1}) and the dependence of the oxidation peak current density (at 0.6 V) of glucose on scan rate (left inset).

diffusion-controlled, which is in good agreement with earlier similar work.[36,37]

To evaluate the selectivity of the Cu−Cu_2O/TiO_2 NTA/Ti electrode, we examined the current responses to several possible interfering biomolecules, such as ascorbic acid (AA), uric acid (UA), and fructose (which normally coexist with glucose in human blood), as shown in Figure S4 in the Supporting Information. Considering that the concentration of glucose in human blood is more than 30 times that of interfering materials,[14] the interference experiment was conducted at the Cu−Cu_2O/TiO_2 NTA/Ti electrode by the successive addition of 1.0 mM glucose and 0.10 mM interfering materials into the 0.10 M NaOH solution. The results showed an apparent response to glucose and insubstantial responses to interfering materials. Although the Cu-based electrode materials used a very high potential in the biosensor performance, the applied potential of 0.60 V for this study's obtained Cu_2O/TNT NTA/Ti electrodes is not very high compared with the values in the literature.[38] The Cu_2O/TNT NTA/Ti electrode can hence be concluded to demonstrate high selectivity for glucose detection.

Most of the sensors for the nonenzymatic electro-oxidation of glucose based on noble metal are reported to easily lose their activity because of complexation between noble metal and Cl^-, which is abundant in physiological fluids. Thus, the current response of the Cu−Cu_2O/TiO_2 NTA/Ti electrode was also examined by adding 0.2 M NaCl to the solution as a supporting electrolyte. The experimental results showed that the peak current of the Cu−Cu_2O/TiO_2 NTA/Ti electrode toward oxidation of glucose remained almost unchanged, and the starting oxidation potential for the electrode in the NaCl solution was even lower than that in the absence of NaCl solution (Figure S5 in the Supporting Information), indicating that the electrode is hardly poisoned by chloride ions. The sensor property of the electrode is even improved due to the addition of NaCl solution.

3.5. Discussion. We reported the first fabrication of Cu−Cu_2O nanoparticles on the surface of TiO_2 NTA as a transducer for the direct electrocatalytic oxidation of the sensor. Our results and those of other glucose sensors are shown in Table 6, which compares them on the basis of the type of the sensitivity, linear range of detection, limit of detection, and detection potential. The sensitivity of the Cu−Cu_2O/TiO_2 NTA/Ti electrode is higher than that of other previously reported glucose sensors based on TiO_2 NT arrays, Cu, and Cu_xO-based nanostructures (Table 6).

Although a nonenzymatic glucose sensor, based on the Cu_2O polyhedron covered with Cu foil on single-walled carbon nanotubes (SWCNT), presented the highest sensitivity of 3029 $\mu A\ cm^{-2}\ mM^{-1}$ in previous work,[39] we have achieved a dramatic increase in sensitivity up to 4895 $\mu A\ cm^{-2}\ mM^{-1}$ by depositing Cu and Cu_2O onto the TiO_2 nanotubes at higher deposition potentials. The improved sensitivity is correlated with the favorable band alignment of the overall structure, preferring electron flow from the absorber Cu and Cu_2O to the TiO_2 nanotubes.

Cu metal cooperated with Cu_2O to form a cocatalyst that may facilitate the transportation of electrons, thus enhancing the property of glucose nonenzymatic electro-oxidation. Moreover, helical TiO_2 nanotube arrays have good conductivity due to defects in their structure that promote the electron transfer reactions of various molecules. Furthermore, the behavior of Cu−Cu_2O and TiO_2−Ti is analogous to characteristics of two semiconductor/metal Schottky barrier diodes. The characteristics enhance the rapid transport of surface reaction electrons to the metal substrate, thereby enhancing the performance of nonenzymatic biosensors.[40]

More importantly, the detailed differences among the electrodes obtained at different electroplating potentials are related to the band models of Cu_2O and TiO_2. The band structure matching Cu_2O particles and anatase TiO_2 enhances the surface reaction electron transfer through the bands of the oxides. The property differences of these Cu−Cu_2O/TiO_2 NTA/Ti electrodes have been well explained by EIS. For the

Table 6. Sensing Characteristics of Cu and Cu_xO Based on Nonenzymatic Glucose Sensors

electrode	sensitivity ($\mu A\ cm^{-2}\ mM^{-1}$)	linear range (mM)	detection limit	detection potential	references
Cu_2O nanospindles and MWCNTs	2143	0.5 μ−2.5	0.2 μM	0.40 V vs SCE	6
CuO−SWCNT	1.61	0.05 μ to 1.8	50 nM	0.45 V vs SCE	41
Cu_2O−C Vulcan XC-72	629	up to 3	2.4 μM	0.75 vs Hg−HgO	42
Cu_2O−Cu	3029	10 μ−0.53	3 μM	0.45 V	39
Cu−Cu_2O nanoporous NPs	123.8	0.01−5	0.05 μM	0.6 V vs SCE	43
Cu−PPy nanowires	180.65	0.1−0.8	1 μM	0.7 V vs SCE	44
CuO/TiO_2	79.79	up to 2.0	1 μM	0.50 V vs SCE	14
NiO/TiO_2	252.0	0.005−12.1	1.0 μM	0.47 V vs SCE	45
Cu_2O/TiO_2	14.56	3−9	62 μM	0.65 V vs SCE	our previous work (3)
Cu−Cu_2O/TiO_2	4895	0.1−2.5	8.6 μM	0.65 V vs SCE	this work

DOI: 10.1021/acsami.5b03401
ACS Appl. Mater. Interfaces 2015, 7, 12719−12730

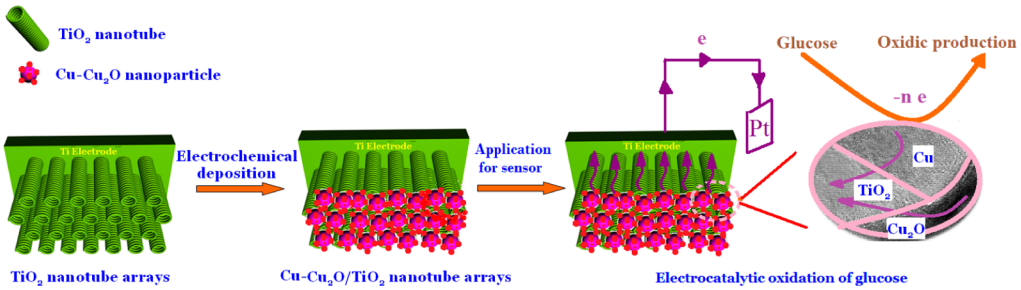

Figure 8. A schematic illustration of the preparation of the Cu−Cu_2O/TiO_2 NTA/Ti electrode and the electron transfer through the Cu−Cu_2O/TiO_2 TNA interface for the electrocatalytic oxidation of glucose.

case of the electrode prepared at −1.0 V, the lowest Rct in Table2 could be attributed to the formation of Cu_2O−TiO_2 heterostructures with higher charge separation efficiency due to the good conductivity of Cu−Cu_2O with octahedral morphology. The Cu−Cu_2O/TiO_2 NTA electrode with a lower Rct indicated that an efficient electrical network through Cu−Cu_2O nanoparticles directly anchoring on the surface of TiO_2 NTA facilitates electron transfer. Nonenzymatic electro-oxidation of glucose is greatly enhanced due to blending Cu and Cu_2O compared with that of the CuO/TiO_2 electrodes.[14]

With an applied positive bias potential, the electrons traveled vectorally along Cu_2O and Cu to the long axis of TiO_2 nanotubes and passed the TiO_2−Ti interface to the external circuit as shown in Figure 8. As a result, the electro-oxidation rate of glucose was greatly improved.

Another way to improve the sensor performance is to optimize its crystal growth and components such that the grains are small enough to offer as little resistance as possible for the electron delivery. The evidence for particle size sensitivity is clear, and in our own experiments with TiO_2 nanotubes (approximately 105 nm) that deposited Cu_2O and Cu nanoparticles (approximately 20 nm), evident improvement in performance was observed. Careful tuning of the Cu_2O and Cu deposition process is required to achieve a balance between covering the surface of TiO_2 nanotubes with sufficiently small Cu_2O and Cu, and maintaining the suitable ratio of Cu_2O and Cu: small particles increase the effective interfacial area, whereas great amounts of Cu_2O appears to result in a broad linear range. According to Ortiz's assumption,[29] the crucial factor for glucose oxidation at the Cu-based electrode in the alkaline solution is the formation of CuOOH species; any conditions favoring this process enhance glucose oxidation,[30] so the presence of a suitable ratio of Cu_2O to Cu in Cu−Cu_2O/TiO_2 NTA/Ti electrodes enhances the formation of CuOOH and accordingly delivers a high steady-state-oxidation current density and better sensitivity. Therefore, the high sensitivity was attributed to the synergistic effect of the small Cu−Cu_2O grain size and the large surface area of the helical TiO_2 nanotube arrays as well as the fast electron transfer.

4. CONCLUSIONS

(a) A nonenzyme glucose sensor was developed for the first time by a simple and controllable electrodeposition method at a deposition potential range from −1.0 to −1.6 V. The helical TiO_2 NTA with a tube diameter of about 105 nm were prepared by anodic oxidation, and a Cu and Cu_2O mixture layer with an approximate thickness of several hundreds of nanometers was electrodeposited on the surface of the TiO_2 NTA. The fabricated Cu−Cu_2O/TiO_2 NTA/Ti electrodes showed excellent electrocatalytic activity and much higher sensitivity toward the oxidation of nonenzymatic glucose. (b) The effects of the detailed fabricating conditions on the performance of nonenzymatic glucose oxidation over the Cu−Cu_2O/TiO_2 NTA/Ti electrode were investigated. (c) The nonenzymatic glucose sensing properties of the Cu−Cu_2O/TiO_2 NTA/Ti electrodes showed a higher sensitivity (4895 $\mu A\ cm^{-2}\ mM^{-1}$) toward glucose oxidation due to the large surface area of the highly dispersed Cu and Cu_2O nanoparticles for electrocatalytic reaction and the fast electron transfer in the Cu−Cu_2O/TiO_2 NTA/Ti electrode. The good sensor performance, low cost, and simple preparation method make this novel electrode material promising for the development of effective glucose sensors for direct electrocatalytic oxidation, which might find promising applications in biological fuel cells.

■ ASSOCIATED CONTENT

Supporting Information

Additional characterization figures including XRD patterns and SEM images of the annealing treatment and figures showing the amperometric responses and CVs of electrodes. The Supporting Information is available free of charge on the ACS Publications website at DOI: 10.1021/acsami.5b03401.

■ AUTHOR INFORMATION

Corresponding Author

*Tel: +86-731-8887-9616. Fax: +86-731-8887-9616. E-mail: tangaidong@126.com, adtang@csu.edu.cn.

Author Contributions

#These authors contributed equally to the research.

Notes

The authors declare no competing financial interest.

■ ACKNOWLEDGMENTS

The authors gratefully acknowledge financial assistance from the National Natural Science Foundation of China (no. 51374250) and the Hunan Provincial Natural Science Foundation for Innovative Research Groups (no. 2013-02).

■ REFERENCES

(1) Clark, L. C.; Lyons, C. Electrode Systems for Continuous Monitoring in Cardiovascular Surgery. *Ann. N.Y. Acad. Sci.* **1962**, *102*, 29−45.

(2) Updike, S. J.; Hicks, G. P. The Enzyme Electrode. *Nature* **1967**, *214*, 986−988.

(3) Long, M.; Tan, L.; Liu, H. T.; He, Z.; Tang, A. D. Novel Helical TiO_2 Nanotube Arrays Modified By Cu_2O for Enzyme-Free Glucose Oxidation. *Biosens. Bioelectron.* **2014**, *59*, 243−250.

DOI: 10.1021/acsami.5b03401
ACS Appl. Mater. Interfaces 2015, 7, 12719−12730

(4) Guo, S. J.; Wang, E. K. Noble Metal Nanomaterials: Controllable Synthesis and Application in Fuel Cells and Analytical Sensors. *Nano Today* **2011**, *6*, 240−264.
(5) Hosseini, M. G.; Momeni, M. M. Platinum Nanoparticle-Decorated TiO_2 Nanotube Arrays as New Highly Active and Non-Poisoning Catalyst for Photo-Electrochemical Oxidation of Galactose. *Appl. Catal., A* **2012**, *427*, 35−42.
(6) Hu, Q. Y.; Wang, F. Y.; Fang, Z.; Liu, X. W. Cu_2O−Au Nanocomposites for Enzyme-Free Glucose Sensing with Enhanced Performances. *Colloids Surf., B* **2012**, *95*, 279−283.
(7) Pasta, M.; La Mantia, F.; Cui, Y. Mechanism of Glucose Electrochemical Oxidation on Gold Surface. *Electrochim. Acta* **2010**, *55*, 5561−5568.
(8) Yu, S. J.; Peng, X.; Cao, G. Z.; Zhou, M.; Qiao, L.; Yao, J. Y.; He, H. C. Ni Nanoparticles Decorated Titania Nanotube Arrays as Efficient Nonenzymatic Glucose Sensor. *Electrochim. Acta* **2012**, *76*, 512−517.
(9) Pissinis, D. E.; Sereno, L. E.; Marioli, J. M. Characterization of Glucose Electro-oxidation at Ni and Ni−Cr Alloy Electrodes. *J. Electroanal. Chem.* **2013**, *694*, 23−29.
(10) Si, P.; Huang, Y. J.; Wang, T. H.; Ma, J. M. Nanomaterials for Electrochemical Non-Enzymatic Glucose Biosensors. *RSC Adv.* **2013**, *3*, 3487−3502.
(11) Park, S.; Chung, T. D.; Kim, H. C. Nonenzymatic Glucose Detection Using Mesoporous Platinum. *Anal. Chem.* **2003**, *75*, 3046−3049.
(12) Li, S. J.; Xia, N.; Lv, X.-L.; Zhao, M. M.; Yuan, B.-Q.; Pang, H. A Facile One-Step Electrochemical Synthesis of Graphene/Nio Nanocomposites as Efficient Electrocatalyst for Glucose and Methanol. *Sens. Actuators, B* **2014**, *190*, 809−817.
(13) Tung, S. P.; Huang, T. K.; Lee, C. Y.; Chiu, H. T. Electrochemical Growth of Gold Nanostructures on Carbon Paper for Alkaline Direct Glucose Fuel Cell. *RSC Adv.* **2012**, *2*, 1068−1073.
(14) Luo, S. L.; Su, F.; Liu, C. B.; Li, J. X.; Liu, R. H.; Xiao, Y.; Li, Y.; Liu, X. N.; Cai, Q. Y. A New Method for Fabricating a CuO/TiO_2 Nanotube Arrays Electrode and Its Application as A Sensitive Nonenzymatic Glucose Sensor. *Talanta* **2011**, *86*, 157−163.
(15) Meng, F. H.; Shi, W.; Sun, Y. N.; Zhu, X.; Wu, G. S.; Ruan, C. Q.; Liu, X.; Ge, D. T. Nonenzymatic Biosensor Based on Cu_xO Nanoparticles Deposited on Polypyrrole Nanowires for Improving Detection Range. *Biosens. Bioelectron.* **2013**, *42*, 141−147.
(16) Zhou, X. M.; Nie, H. G.; Yao, Z.; Dong, Y. Q.; Yang, Z.; Huang, S. M. Facile Synthesis of Nanospindle-Like Cu_2O/Straight Multi-Walled Carbon Nanotube Hybrid Nanostructures and Their Application in Enzyme-Free Glucose Sensing. *Sens. Actuators, B* **2012**, *168*, 1−7.
(17) Xiang, J. Y.; Tu, J. P.; Yuan, Y. F.; Huang, X. H.; Zhou, Y.; Zhang, L. Improved Electrochemical Performances of Core-Shell Cu_2O/Cu Composite Prepared by a Simple One-Step Method. *Electrochem. Commun.* **2009**, *11*, 262−265.
(18) Mor, G. K.; Varghese, O. K.; Paulose, M.; Shankar, K.; Grimes, C. A. A Review on Highly Ordered, Vertically Oriented TiO_2 Nanotube Arrays: Fabrication, Material Properties, and Solar Energy Applications. *Sol. Energy Mater. Sol. Cells* **2006**, *90*, 2011−2075.
(19) Zhang, X. C.; Yang, H. M.; Tang, A. D. Optical, Electrochemical and Hydrophilic Properties of Y_2O_3 Doped TiO_2 Nanocomposite Films. *J. Phys. Chem. B* **2008**, *112*, 16271−16279.
(20) Yang, H. M.; Zhang, K.; Shi, R. R.; Tang, A. D. Sol-Gel Synthesis And Photocatalytic Activity of CeO_2/TIO_2 Nanocomposites. *J. Am. Ceram. Soc.* **2007**, *90*, 1370−1374.
(21) Huang, L.; Zhang, S.; Peng, F.; Wang, H.; Yu, H.; Yang, J.; Zhang, S.; Zhao, H. Electrodeposition Preparation of Octahedral-Cu_2O-Loaded TiO_2 Nanotube Arrays for Visible Light-Driven Photocatalysis. *Scr. Mater.* **2010**, *63*, 159−161.
(22) Tang, A. D.; Deng, Y. H.; Jin, J.; Yang, H. M. $ZnFe_2O_4$-TiO_2 Nanoparticles within Mesoporous MCM-41. *Sci. World J.* **2012**, *1*, 1−5.
(23) Wang, M. Y.; Sun, L.; Lin, Z. Q.; Cai, J. H.; Xie, K. P.; Lin, C. J. p-n Heterojunction Photoelectrodes Composed of Cu_2O-loaded TiO_2 Nanotube Arrays with Enhanced Photoelectrochemical and photoelectrocatalytic activities. *Energy Environ. Sci.* **2013**, *6*, 1211−1220.
(24) Foo, W. J.; Zhang, C.; Ho, G. W. Non-noble metal Cu-loaded TiO_2 for enhanced photocatalytic H_2 production. *Nanoscale* **2013**, *5*, 759−764.
(25) Yu, J. G.; Ran, J. R. Facile preparation and Enhanced Photocatalytic H_2-Production Activity of $Cu(OH)_2$ Cluster Modified TiO_2. *Energy Environ. Sci.* **2011**, *4*, 1364−1371.
(26) Xing, J.; Chen, Z. P.; Xiao, F. Y.; Ma, X. Y.; Wen, C. Z.; Li, Z.; Yang, H. G. Cu−Cu_2O−TiO_2 Nanojunction Systems with an Unusual Electron-Hole Transportation Pathway and Enhanced Photocatalytic Properties. *Chem.—Asian J.* **2013**, *8*, 1265−1270.
(27) Li, Z. H.; Liu, J. W.; Wang, D. J.; Gao, Y.; Shen, J. Cu_2O/Cu/TiO_2 Nanotube Ohmic Heterojunction Arrays with Enhanced Photocatalytic Hydrogen Production Activity. *Int. J. Hydrogen Energy* **2012**, *37*, 6431−6437.
(28) Zhao, L.; Dong, W.; Zheng, F. G.; Fang, L.; Shen, M. R. Interrupted Growth and Photoelectrochemistry of Cu_2O and Cu Particles On TiO_2. *Electrochim. Acta* **2012**, *80*, 354−361.
(29) Ortiz, R.; Márquez, O. P.; Márquez, J.; Gutiérrez, C. Necessity of Oxygenated Surface Species for the Electrooxidation of Methanol on Iridium. *J. Phys. Chem.* **1996**, *100*, 8389−8396.
(30) Hassan, H. B.; Abdel Hamid, Z. Electrodeposited Cu−CuO Composite Films for Electrochemical Detection of Glucose. *Int. J. Electrochem. Sci.* **2011**, *6*, 5741−5758.
(31) Wang, J.; Ji, G.; Liu, Y.; Gondal, M. A.; Chang, X. Cu_2O/TiO_2 Heterostructure Nanotube Arrays Prepared by an Electrodeposition Method Exhibiting Enhanced Photocatalytic Activity for CO_2 Reduction to Methanol. *Catal. Commun.* **2014**, *46*, 17−21.
(32) Zhang, S.; Zhang, S.; Peng, F.; Zhang, H.; Liu, H.; Zhao, H. Electrodeposition of Polyhedral Cu_2O on TiO_2 Nanotube Arrays for Enhancing Visible Light Photocatalytic Performance. *Electrochem. Commun.* **2011**, *13*, 861−864.
(33) Yang, H. M.; Zhang, X. C.; J, O. *Low-Dimensional Metal Oxide Nanomaterials*. Science Press, Beijing, 2012, p. 18.
(34) Pauliukaite, R.; Ghica, M. E.; Fatibello-Filho, O.; Brett, C. M. A. Electrochemical Impedance Studies of Chitosan-Modified Electrodes for Application in Electrochemical Sensors and Biosensors. *Electrochim. Acta* **2010**, *55*, 6239−6247.
(35) Shervedani, R. K.; Bagherzadeh, M. Electrochemical Impedance Spectroscopy as a Transduction Method for Electrochemical Recognition of Zirconium on Gold Electrode Modified with Hydroxamated Self-Assembled Monolayer. *Sens. Actuators, B* **2009**, *139*, 657−664.
(36) Zhuang, Z. J.; Su, X. D.; Yuan, H. Y.; Sun, Q.; Xiao, D.; Choi, M. M. F. An Improved Sensitivity Non-Enzymatic Glucose Sensor Based on a CuO Nanowire Modified Cu Electrode. *Analyst (Cambridge, U. K.)* **2008**, *133*, 126−132.
(37) Babu, T. G. S.; Ramachandran, T.; Nair, B. Single Step Modification of Copper Electrode for The Highly Sensitive and Selective Non-Enzymatic Determination of Glucose. *Microchim. Acta* **2010**, *169*, 49−55.
(38) Zhang, P.; Zhang, L.; Zhao, G. C.; Feng, F. A Highly Sensitive Nonenzymatic Glucose Sensor Based on CuO Nanowires. *Microchim. Acta* **2012**, *176*, 411−417.
(39) Luo, Z. J.; Han, T. T.; Qu, L. L.; Wu, X. Y. A Ultrasensitive Nonenzymatic Glucose Sensor Based on Cu_2O Polyhedrons Modified Cu Electrode. *Chin. Chem. Lett.* **2012**, *23*, 953−956.
(40) Wang, C.; Yin, L.; Zhang, L.; Gao, R. Ti/TiO_2 Nanotube Array/Ni Composite Electrodes for Nonenzymatic Amperometric Glucose Sensing. *J. Phys. Chem. C* **2010**, *114*, 4408−4413.
(41) Dung, N. Q.; Patil, D.; Jung, H.; Kim, D. A High-Performance Nonenzymatic Glucose Sensor Made of CuO−SWCNT Nanocomposites. *Biosens. Bioelectron.* **2013**, *42*, 280−286.
(42) El Khatib, K.; Abdel Hameed, R. Development of Cu_2O/Carbon Vulcan XC-72 as Non-Enzymatic Sensor for Glucose Determination. *Biosens. Bioelectron.* **2011**, *26*, 3542−3548.

DOI: 10.1021/acsami.5b03401
ACS Appl. Mater. Interfaces 2015, 7, 12719−12730

(43) Zhao, Y. X.; Li, Y. P.; He, Z. Y.; Yan, Z. F. Facile Preparation of Cu−Cu_2O Nanoporous Nanoparticles as a Potential Catalyst for Non-Enzymatic Glucose Sensing. *RSC Adv.* **2013**, *3*, 2178−2181.
(44) Liu, Y.; Liu, Z.; Lu, N.; Preiss, E.; Poyraz, S.; Kim, M. J.; Zhang, X. Facile Synthesis of Polypyrrole Coated Copper Nanowires: A New Concept to Engineered Core-Shell Structures. *Chem. Commun.* **2012**, *48*, 2621−2623.
(45) Yu, J.-G.; Yu, L.-Y.; Yang, H.; Liu, Q.; Chen, X.-H.; Jiang, X.-Y.; Chen, X.-Q.; Jiao, F.-P. Graphene Nanosheets as Novel Adsorbents in Adsorption, Preconcentration and Removal of Gases, Organic Compounds and Metal Ions. *Sci. Total Environ.* **2015**, *502*, 70−79.

DOI: 10.1021/acsami.5b03401
ACS Appl. Mater. Interfaces 2015, 7, 12719−12730